High-speed RNA microextraction technology using magnetic oligo-dT beads and lateral magnetophoresis†

Hwanyong Lee, Jinhee Jung, Song-I Han and Ki-Ho Han*

Received 19th April 2010, Accepted 19th July 2010
DOI: 10.1039/c005145d

This paper presents a high-speed RNA microextractor for the direct isolation of RNA from peripheral blood lysate using magnetic oligo-dT beads. The extraction is achieved through lateral magnetophoresis, generated by a ferromagnetic wire array inlaid on a glass substrate. This RNA microextractor separated more than 80% of magnetic beads with a flow rate up to 20 ml h^{-1}, and the overall extraction procedure was completed within 1 min. The absorbance ratio of RNA to protein (A_{260}/A_{280}) was >1.7, indicating that the extraction technology yielded nearly pure RNA. The feasibility of this technique was evaluated further for its applicability to reverse transcription polymerase chain reaction (RT-PCR) procedures by performing cDNA synthesis and PCR. The analysis verified that the RNA microextractor is a practical method for easy, rapid, and high-precision RT-PCR using minimal reagent volumes without requiring highly trained personnel. In addition, it can be readily incorporated into genetic analysis procedures for realizing automated on-chip genetic platforms in a micro format.

1. Introduction

Reverse transcription polymerase chain reaction (RT-PCR) is a powerful genetic analysis technique for measuring gene expression, which can be applied to medical diagnostics[1–3] and forensics.[4,5] The extraction of high-quality RNA from crude biological samples is critical to obtain rapid and accurate RT-PCR performance. RNA is readily destroyed by ribonucleases (RNases), which are produced by bacteria and molds present on human skin and are found in dust in the environment. As the ubiquitous RNases are highly active enzymes, it is difficult to extract high-quality RNA without contamination and degradation by RNases.

Conventional procedures for nucleic acid isolation are generally performed using silica-based solid-phase extraction,[6–11] the efficiency of which depends on the interaction between the nucleic acid and the solid support in the presence of a chaotropic salt buffer. In the conventional procedure, a crude biological sample is lysed and then loaded onto the solid support where the RNA binds. Subsequently, other unwanted lysate components, such as lipids, proteins, small molecule metabolites, and inorganic ions, are washed away and then the bound RNA is released from the support using a solution with low ionic strength. This exposes purified RNA to the outside environment, risking contamination by RNases at any step in the extraction procedure. RNases can be particularly problematic contaminants because they are difficult to inactivate. Thus, to avoid contamination and degradation by RNases, a closed, RNase-free, rapid RNA extraction method is essential for obtaining high-quality RNA for downstream RT-PCR processes. To achieve this, microchip-based devices[12–17] have been developed with a closed format to prevent RNase contamination and an integrated format for obtaining high-quality RNA without the need for highly trained personnel.

In this report, we introduce a high-speed RNA microextraction technology using magnetic oligo-dT beads (Dynabeads® oligo $(dT)_{25}$; Invitrogen Dynal AS, Oslo, Norway)[18] and lateral magnetophoresis.[19] The lateral magnetic force is generated using a ferromagnetic wire array inlaid on a glass substrate. An analytical model of the lateral magnetic force was derived to estimate the lateral displacement of magnetic beads passing over the ferromagnetic wires and was verified by comparison with numerical results. Quantitative measurements of the separation efficiency of the magnetic beads and the purities of the extracted RNA samples at various flow rates are reported. RT-PCR amplification of a 219-bp fragment of the human β-actin gene demonstrated that the extracted RNA sample was of sufficient quality for direct use in RT-PCR.

2. Theory and design

2.1 Working principle

A uniform external magnetic field normal to the axis of a ferromagnetic wire is deformed near the wire, where a high-gradient magnetic field appears. Thus, magnetic beads placed near a ferromagnetic wire experience a magnetic force. Consider a ferromagnetic wire array placed at an angle of θ to the direction of flow (Fig. 1A) and inlaid over the whole area of a microchannel (Fig. 1B). When an external magnetic field is applied, the inlaid ferromagnetic wire array generates a high-gradient magnetic field over the whole area of the microchannel. Then, magnetic beads passing over the wire experience magnetic force F_m with hydrodynamic drag force F_d (Fig. 1A). The lateral magnetic force, F_l, on a bead is the vector sum of the magnetic force and the drag force. As the lateral magnetic force is generated regularly over the whole area of the microchannel, the proposed microextractor would potentially have a greater

School of Nano Engineering, Inje University, 607 Obang-dong, Gimhae, GyongNam, 621-749, Republic of Korea. E-mail: mems@inje.ac.kr; Fax: +82-55-320-3715; Tel: +82-55-320-3715

† Electronic supplementary information (ESI) available: Supplementary equations and figures. See DOI: 10.1039/c005145d

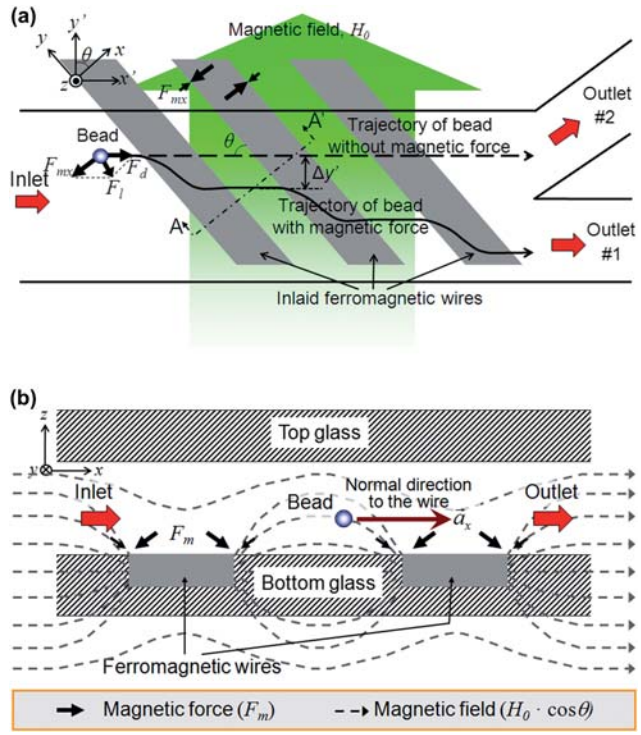

Fig. 1 Working principle of the high-speed RNA microextractor. (A) Top view of the inlaid ferromagnetic wire array placed at an angle of θ relative to the direction of flow under an applied external magnetic field H_0. Magnetic force on the magnetic beads is induced by a high-gradient magnetic field generated near the ferromagnetic wire array with an external magnetic field. Lateral displacement is created by the magnetic force F_m and hydrodynamic drag force F_d. (B) Cross-sectional view of the ferromagnetic wire array and the gradient magnetic field along the A–A' cross-section in Fig. 1A.

separation efficiency and throughput than previous magnetophoretic microseparators,[20,21] which use only a single ferromagnetic wire. The lateral magnetic force is determined by the magnitude of magnetic force F_m depending on the strength of the applied external magnetic field, the relative magnetic susceptibility of the beads, and the angle between the wire and the direction of flow. Lateral displacement is created by the lateral magnetic force and can therefore be controlled by the angle. Consequently, with an external magnetic field, the magnetic beads are forced laterally and flow into outlet #1, and other components in the crude lysate sample wash out through outlet #2 (Fig. 1A). As a result, with on external magnetic field, the beads flow into outlet #2 along with the rest of the lysate.

2.2 Analytical and numerical simulations

The x-directional magnetic force F_{mx} in Fig. 1A, which acts on a magnetic bead near the ferromagnetic wire, is expressed as follows (see Electronic supplementary information [ESI†] for more detailed descriptions):

$$F_{mx} = -\frac{2V_P M_{PS} x k a^2 B_0}{(x^2+z^2)^2\sqrt{(x^2+z^2)^2+2ka^2(x^2-z^2)+k^2a^4}} \quad (1)$$

$$\left(x^2-3z^2+ka^2\right),\ k=\frac{\mu_W-\mu_B}{\mu_W+\mu_B}$$

where V_P represents the volume of the magnetic bead, M_{PS} is the saturation magnetization of the beads, μ_B is the permeability of the buffer solution, μ_W is the permeability of the ferromagnetic wire, a is the effective radius of the ferromagnetic wire, B_0 is the applied external magnetic flux, and x and z are the axes of the Cartesian coordinate system.

The saturation magnetization M_{PS} of the magnetic beads used for analytical and numerical simulations was 30 kA m^{-1}.[22] The external magnetic flux, $B_0 = \mu_0 H_0$, generated by a permanent magnet was measured as 0.14 T using a Gauss/Tesla-meter (Model 9550; F.W. Bell). The x-directional magnetic force on the magnetic bead was analyzed and compared with that of a numerical simulation using the commercial finite element code ANSYS (ANSYS Inc.) (Fig. 2A). The numerical magnetic force from a square wire was slightly greater than the analytical value from a circular wire. To compensate for this difference, a correction factor of $4/\pi$ was used, which is the ratio of cross-sectional area between the square and circular wires.[20] The analytical magnetic force from the circular wire should be multiplied by the correction factor to estimate the magnetic force of the square wire. The corrected magnetic forces from the circular wire (radius = 5 μm) agreed well with the numerical values from the square wire (10 × 10 μm^2) (Fig. 2A). Thus, the comparison demonstrated that the derived analytical model was useful for estimating the magnetic force acting on the magnetic bead in the RNA microextractor.

The total lateral force vector $\vec{F}_l$ (Fig. 1A) on the magnetic bead becomes

$$\vec{F}_l = \vec{F}_{mx} + \vec{F}_d = (F_{mx} + F_d \sin\theta)\,\vec{a}_x - F_d \cos\theta\,\vec{a}_y \quad (2)$$

where $\vec{F}_d$ represents the hydrodynamic drag force on a magnetic bead. The lateral velocity of the magnetic bead, $\vec{v}_l$ is

$$\vec{v}_l = \frac{\vec{F}_l}{6\pi\eta d} = \beta\left[(F_{mx} + F_d \sin\theta)\,\vec{a}_x - F_d \cos\theta\ \vec{a}_y\right],\ \beta = \frac{1}{6\pi\eta d} \quad (3)$$

where η represents the apparent viscosity of the magnetic beads in the medium and d is the radius of the magnetic beads. If the levitation height z is constant, then the x- and y-directional displacements are

$$dx = \beta(F_{mx} + F_d \sin\theta)\,dt \quad (4)$$

$$y = -\beta F_d \cos\theta\ t \quad (5)$$

Using the analytical results x and y of eqn (4) and (5), the y'-directional lateral displacement $\Delta y'$ (Fig. 1A) of the magnetic beads can be obtained as result of rotation of the reference coordinate system about the z-axis by an angle θ, as follows:

$$\Delta y' = x\cos\theta + y\sin\theta \quad (6)$$

According to eqn (4) and (6), the lateral displacement $\Delta y'$ increases as the magnitude of the x-directional magnetic force F_{mx} on the magnetic bead increases or the angle θ between the ferromagnetic wire and direction of flow decreases. Especially, for $F_{mx} + F_d \sin\theta < 0$ [eqn (4)], the magnetic beads cannot pass over the ferromagnetic wire, and thus the lateral displacement becomes infinite. Then, the magnetic beads will migrate laterally

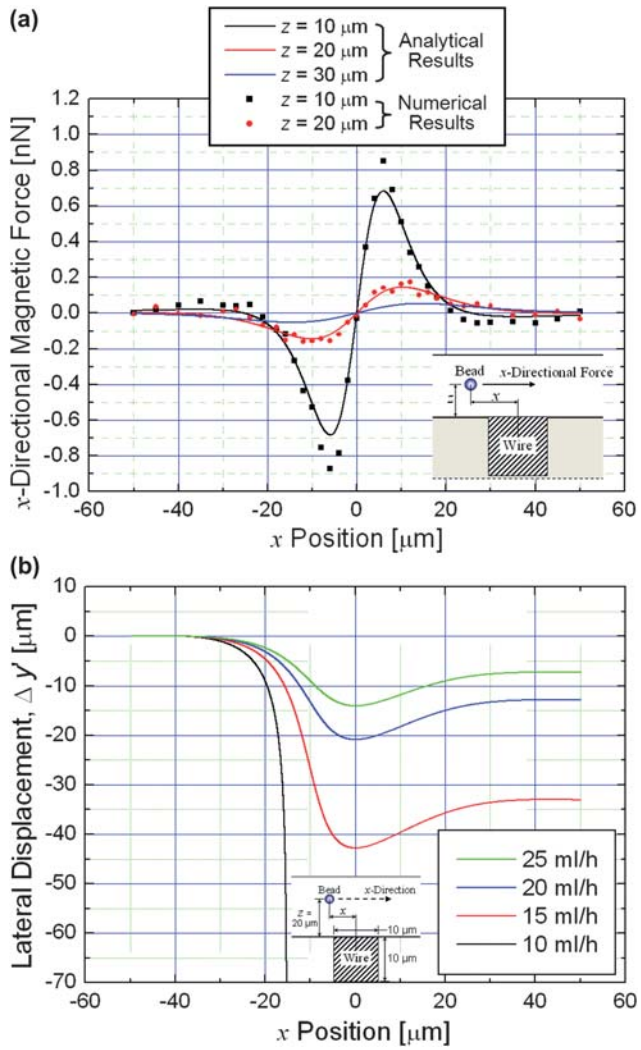

Fig. 2 (A) Analytical and numerical values for the x-directional magnetic force F_{mx} on the magnetic beads for varying levitation height z from the bottom substrate. (B) Analytical values of the lateral displacement $\Delta y'$ for various flow rates in the region of $\theta = 5.7°$ and $z = 20$ μm. The hatched squares in the inset represent the cross-section of the square ferromagnetic wire (10×10 μm^2), taken perpendicular to the x-axis in Fig. 1A.

until they approach the sidewall of the microchannel. In addition, the drag force is reduced as the flow rate decreases, thereby increasing the lateral displacement (Fig. 2B).

2.3 Design

The high-speed RNA microextractor consists of two inlets, two outlets, and a piecewise curved ferromagnetic nickel wire array inlaid on the bottom substrate (Fig. 3). The sample and buffer inlets are used for injecting the crude lysate sample mixed oligo-dT magnetic beads and phosphate buffered saline (PBS) solution, respectively. Outlet #1 was designed for extracting the beads and outlet #2 for removing the rest of the lysate components. To enrich beads, the width of outlet #1 was designed to be 200 μm, one quarter if the width of outlet #2 (800 μm). The width and thickness (50 μm and 10 μm, respectively) of the

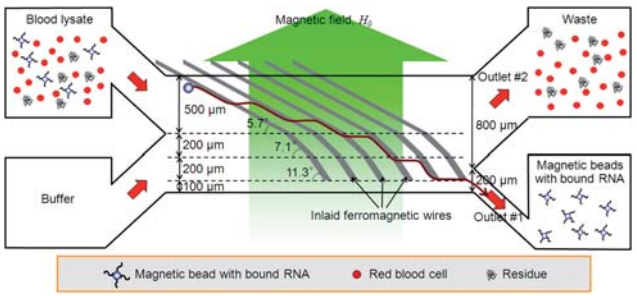

Fig. 3 Architecture of the high-speed RNA microextractor. The ferromagnetic wire array is divided into three regions in which the angles between the ferromagnetic wire and the direction of flow are 5.7°, 7.1°, and 11.3°, respectively. To avoid accumulation of beads at the corners between ferromagnetic wires and the sidewall of the microchannel, the ferromagnetic wire array is patterned 100 μm from the sidewall of the microchannel.

ferromagnetic wire were designed to generate a high-gradient magnetic field.

Due to the induced strong magnetic force, some beads may be stacked on the ferromagnetic wire and lost in the microchannel. To increase the recovery rate of the magnetic beads from the microchannel and to reduce aggregation of the magnetic beads on the sidewall of the microchannel with the permanent magnet, the ferromagnetic wire was designed as a piecewise curve with three bend angles of 5.7°, 7.1°, and 11.3° relative to the direction of flow, and patterned 100 μm from the sidewall of the microchannel (Fig. 3).

3. Experimental

3.1 Materials and methods

To extract RNA, we used magnetic beads 2.8 μm diameter (Dynabeads® oligo(dT)$_{25}$; Invitrogen Dynal AS) with oligo dT sequences on their surface. Before the experiment, a solution containing the magnetic beads was suspended thoroughly in a vial to obtain a uniform brown suspension. Then 100 μl of the solution/suspension, containing 4×10^4 beads μl^{-1} and capable of isolating up to 8 ng μl^{-1} of mRNA, was transferred into a 1.5-ml tube. The beads were washed twice with lysis/binding buffer (Dynabeads mRNA Direct kit; Invitrogen Dynal AS), and placed on ice. Human blood lysate was prepared from 50 μl of finger-prick blood added to 175 μl of leukocyte lysis buffer (Buffer RLT, QIAamp RNA Blood Minikit, Qiagen). The solution containing the washed magnetic beads was removed and the prepared lysate was added to the magnetic beads. The sample solution was mixed by pipetting for 5 min at room temperature to allow the RNA to bind to the beads.

It was not necessary to elute the RNA from the Dynabeads® oligo(dT)$_{25}$ beads for downstream procedures (*e.g.*, solid-phase cDNA synthesis); indeed, RNA bound to the beads was used directly for cDNA synthesis. Briefly, 10× buffer RT (2 μl) and dNTP mix (2 μl), Omniscript reverse transcriptase (2.5 μl) (Omniscript RT Kit; Qiagen), and RNase inhibitor (Qiagen), diluted to 4 units μl^{-1} (1 μl) were mixed by vortexing, centrifuged, and the extracted RNA bound to the beads was added and mixed by pipetting. Then, for synthesizing cDNA, the samples were

incubated at 37 °C for 60 min. The sequences of the forward and reverse primers used to amplify a 219-bp fragment of the human β-actin gene were 5′–GAAACTACCTTCAACTCCATC–3′ and 5′–CGAGGCCAGGATGGAGCCGCC–3′, respectively. The 20-μl PCR mixture contained 4 μl of 5 × Taq-PCR mix (Genotech), 0.25 μl forward and reverse primers (100 μmol μl^{-1}; Genotech), 1 μl of cDNA sample as a template, and 14.5 μl of distilled water. Using a commercial thermocycler (PC808; Astec), standard PCR thermocycling was performed as follows: 94 °C for 5 min, followed by 35 cycles of 94 °C for 30 s, 55 °C for 1 min, and 72 °C for 30 s, followed by a final extension at 72 °C for 7 min. The PCR products were analyzed by 2% agarose (Promega) gel electrophoresis with ethidium bromide (Promega) staining followed by observation under UV light to compare the product sizes using fluorescently-labeled DNA standards, and processed using the ImageJ software (NIH).

3.2 Fabrication process

The microfabrication process for the RNA microextractor used glass slides 0.7 mm thick (Borofloat33 Pyrex, Schott AG) and SU8-to-glass adhesive bonding. To form inlaid grooves for the ferromagnetic wires, a Ti/Cu/Cr seed layer for nickel electroplating was electron-beam evaporated onto a glass substrate. Photoresist (AZ9260; AZ Electronic Materials) was spun and patterned to create micromolds 50 μm thick for ferromagnetic nickel wires (Fig. 4A). Then, ferromagnetic nickel wires 30 μm in thickness were electroplated onto the glass substrate. After removing the photoresist, epoxy adhesive (HE #200; Hyundae Epoxy Chemicals Co.) was poured onto the substrate and cured for 6 h at 85 °C to form a flat surface. Subsequently, the ferromagnetic wire array 10 μm in thickness was formed and inlaid on the glass by mechanical nickel polishing (Fig. 4B). To form the microchannel, a layer of SU-8 2050 photoresist 70 μm thick (MicroChem Corp.) was spun and patterned on the glass, along with an evaporated 1000 Å Cr layer to increase the adhesion between the SU-8 and the glass (Fig. 4C). A drill was used to form reservoirs in the top glass as fluid interconnections. This glass was then bonded to the bottom glass using ultraviolet (UV) adhesive (1187-M; DYMAX Co.) (Fig. 4D). A microfluidic system interface (MSI) fabricated by stereolithography (Viper SI2; 3D Systems) was used to make the microfluidic

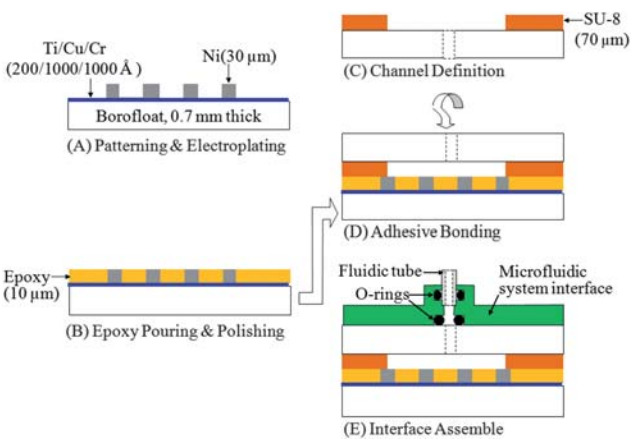

Fig. 4 Fabrication process for the high-speed RNA microextractor.

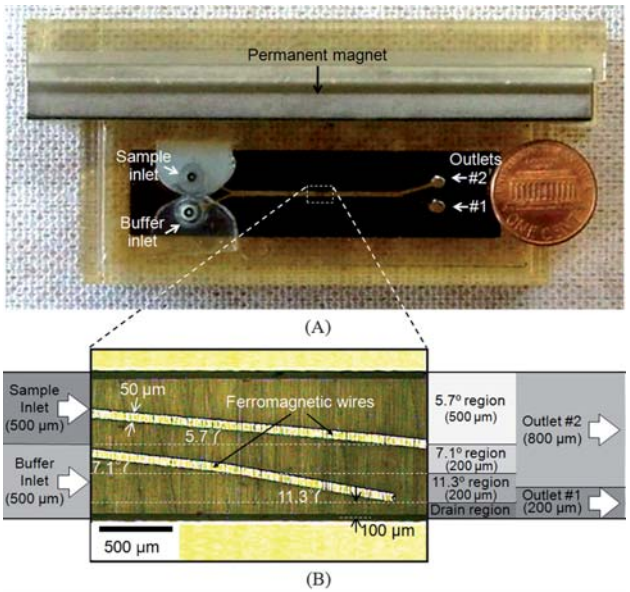

Fig. 5 Photographs of the fabricated high-speed RNA microextractor. (A) Top view of the fabricated high-speed RNA microextractor placed on the alignment jig for aligning the ferromagnetic wire array and the center of the permanent magnet. (B) Enlarged view of the microchannel, which includes the inlaid ferromagnetic wires designed as a piecewise linear curve with three angles of 5.7°, 7.1°, and 11.3° relative to the direction of flow and patterned 100 μm from the sidewall of the microchannel.

interconnections. Nitrile rubber O-rings (Size 001-1/2; McMaster-Carr) were used to seal the microfluidic interconnects. The UV adhesive was dropped into the openings for adhesive bonding on the MSI. Capillary forces pulled the adhesive into the gap between the MSI and the glass chip. The adhesive was cured by placing it under UV light for 30 min, completing the fabrication of the RNA microextractor (Fig. 4E). Fig. 5A and 5B show the fabricated high-speed RNA microextractor. Before the experiment, the RNA microextractor was washed with 2M HCl for 5 min and rinsed with distilled water seven times. To sterilize the RNA microextractor, it was placed under UV light for 5 min.

The instrumental setup for the RNA microextractor included a neodymium iron boron (Nd–Fe–B) permanent magnet and two syringe pumps (KD100; KD Scientific Inc., MA), providing controlled laminar flow in the microchannel. Two 3-ml plastic syringes (BD Biosciences) were connected to the inlets with capillary tubing (Teflon® FER 1/16 in. tubing, 0.25 mm i.d.; Upchurch Scientific). An alignment jig was used to align the ferromagnetic wire to the center of the permanent magnet. If the ferromagnetic wire was not carefully aligned to the center, the external magnetic field was incident to the wire, obliquely resulting in less efficient magnetic coupling and different magnetic forces generated on either side of the ferromagnetic wire.

4. Results and discussion

4.1 Separation efficiency of the magnetic beads

A Nd–Fe–B permanent magnet was used to create an external magnetic flux of 0.14 T. Two syringe pumps were used for

injection of the lysate sample and PBS buffer solution at the same flow rate (from 10 to 25 ml h^{-1}) into the two inlets. The fluids from outlets #1 and #2 were collected during the injection of the sample. The RNA microextractor was placed under a microscope (ME600; Nikon Instruments Inc.) to enable monitoring of the magnetic beads passing over the inlaid ferromagnetic wire array during the experiment. To analyze the separation efficiency of the beads, each solution extracted from outlets #1 and #2 was collected, and the beads in each solution were counted using a hemocytometer (Paul Marienfeld GmbH).

With no external magnetic field, the magnetic beads and lysate in the sample were dispersed uniformly in one half of the microchannel and flowed into outlet #2 (Fig. 6A). On the other hand, when the external magnetic field of 0.14 T was applied, the magnetic beads were drawn laterally and flowed into outlet #1, while the remainder of the lysate still flowed into outlet #2 (Fig. 6B). Fig. 7A shows the separation efficiency of beads extracted from outlet #1 for various sample flow rates from 10 to 25 ml h^{-1}. The RNA microextractor separated more than 80% of the magnetic beads with a flow rate up to 20 ml h^{-1}.

As explained above, as the flow rate decreases, the lateral velocity $\vec{v}_l$ [eqn (3)] decreases; that is, the drag force acting on the magnetic beads decreases and the lateral displacement is therefore increased (Fig. 2B). As a result, the separation efficiency increases as the flow rate decreases (Fig. 7A). Meanwhile, as the flow rate increases, the beads can be freed from stiction to the ferromagnetic wire, thereby increasing the recovery rate. Thus, the flow rate should be controlled appropriately for both the recovery rate and the separation efficiency.

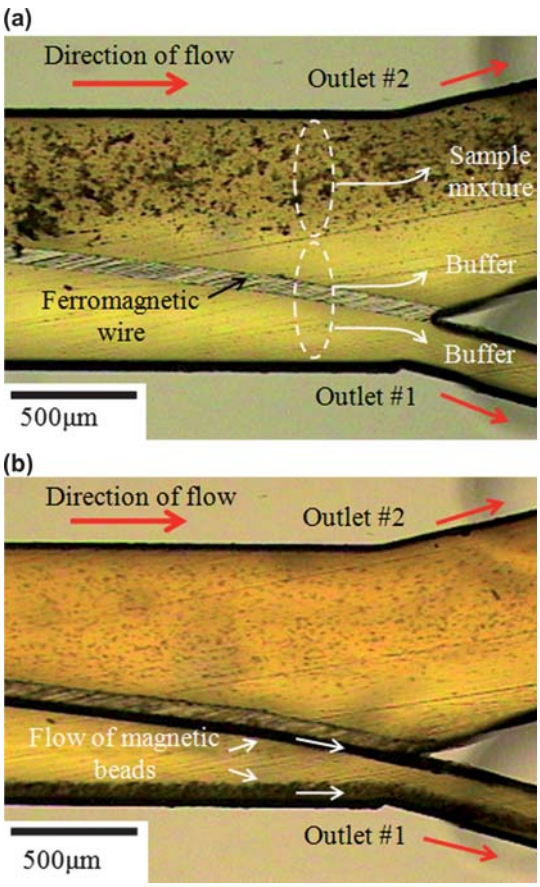

Fig. 6 (A) Sample and buffer solutions pass through the microchannel of the RNA microextractor at sample and buffer flow rates of 15 ml h^{-1}, respectively, without an external magnetic field. In this case, the magnetic beads and other lysate components flow into outlet #2. (B) Sample and buffer solutions pass through the microchannel with an external magnetic flux of 0.14 T. The magnetic beads are laterally drawn and flow into outlet #1, while the other substances flow into outlet #2.

To increase separation throughput and efficiency, the design of the RNA microextractor could be optimized by adjusting the angle (θ) between the wires and the direction of flow, revising the dimensions of the wire, such as width, spacing, and thickness, modifying the geometries of the microchannel, and/or incorporating a ferromagnetic wire with higher permeability, stronger external magnetic field, and 2D/3D structured multiple microchannels.

While passing through the microchannel, the magnetic beads accumulate along the edge of the ferromagnetic wires due to the induced strong magnetic force. Beads at the top of the accumulation are naturally farther away from the wire, and the magnetic force on those beads will therefore be lower than that on other beads. At the same time, because the effective area of the microchannel becomes narrower due to the accumulation, the hydrodynamic drag force on the beads increases and consequently the lateral displacement decreases. For the present RNA microextractor, the lateral displacement was also affected by uncertainties, such as variations in the flow velocity, the height of the microchannel, bead size, bead interactions, and the width of the sample inlet. There was also some error in measurement of the separation efficiency (Fig. 7A) due to inaccuracy of the counting method using a hemocytometer.

A high-gradient magnetic separation method was used to generate a high-gradient magnetic field around the ferromagnetic wire inlaid on the bottom substrate, thereby creating a strong magnetic force on the magnetic beads [eqn (S5)†], and the beads readily showed saturation magnetization. The magnetic force acting on the beads is proportional to the intensity of the external magnetic field, H_0, and the square of the wire thickness, $2a$ [eqn (1)]. The electroplated nickel wire of 10 μm in thickness used here can create a stronger magnetic force than that from a thin wire[23,24] < 2 μm thick fabricated by the metal evaporation method. Thus, even in a weak external magnetic field, the present RNA microextractor can generate a strong magnetic force; in the present study, it was about 0.8 nN (Fig. 2A). Furthermore, due to the ferromagnetic wires inlaid on the glass substrate of the microchannel, the lateral magnetic force was generated regularly over the whole area of the microchannel, and the proposed device therefore has a potentially greater separation efficiency and throughput than previously reported magnetophoretic microseparators,[20,21] which use only a single ferromagnetic wire.

In addition to the x-directional magnetic force, F_{mx} [eqn (1)], there is a vertical, z-directional magnetic force, F_{mz} [eqn (S9)†], pulling the magnetic beads toward the bottom of the microchannel (Fig. S2†). According to analytical and numerical results (Fig. S3†), the maximum vertical magnetic force on a magnetic bead (Dynabeads® oligo$(dT)_{25}$; 2.8 μm diameter) at a levitation height of 10 μm is about 0.3 nN toward the bottom, which is generated by a high-gradient magnetic field of about 150 T m^{-1} around the edge of the ferromagnetic wires. Thus, the magnetic beads located around the edge of the ferromagnetic wires are

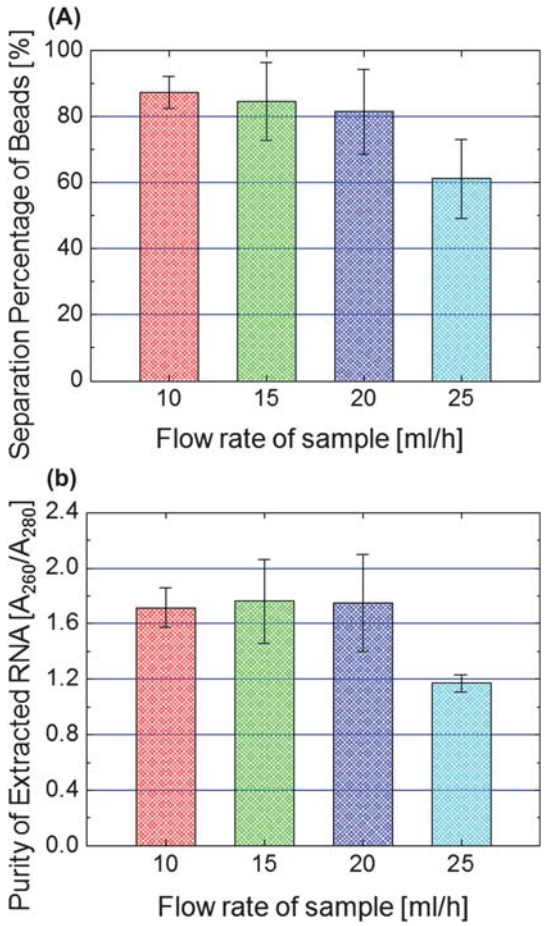

Fig. 7 (A) Relative separation percentage of the beads extracted from outlet #1 with various sample flow rates. The error bars represent one standard deviation calculated from three data sets. (B) Purity of the RNA preparation for various sample flow rates. The error bars represent one standard deviation calculated from three data sets.

forced toward the bottom by the vertical magnetic force. As the beads approach the ferromagnetic wire, the lateral and vertical magnetic forces increase simultaneously, and consequently, the lateral displacement increases.

4.2 RNA purity test

The blood lysate contains not only nucleic acids, but also proteins, lipids, small-molecule metabolites, and inorganic ions. All of these compounds may bind to the magnetic beads or interfere with RNA binding to the surface of the beads. As some of these substances may also act as inhibitors in genetic analysis procedures, such as PCR and nucleotide sequencing,[25] the extraction of high-purity RNA from the crude lysate is critical for the reliability of subsequent genetic analyses. To measure the purity of the extracted product, the RNA bound to the magnetic beads was eluted. Elution buffer (10mM Tris-HCl, Dynabeads mRNA Direct kit, Invitrogen Dynal AS) was added to the extracted solution at a ratio of 1 : 1. Then the eluted RNA was incubated at 75 °C for 2 min. A tube containing RNA was placed on a magnet and the supernatant containing the RNA was transferred quickly to a new tube. The purity of the eluted RNA was assessed using a spectrophotometer (GeneQuant Pro; Amersham Biosciences) (Fig. 7B). The average absorbance ratio of RNA to protein (A_{260}/A_{280}) was greater than 1.7 with a sample flow rate up to 20 ml h^{-1}, indicating that the extracted RNA was sufficiently pure for RT-PCR procedures.[26]

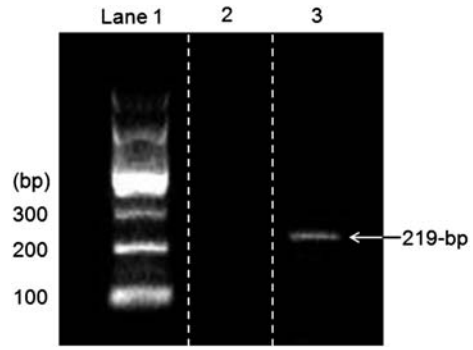

Fig. 8 RT-PCR results using human blood lysate RNA extracted from the RNA microextractor. The RT-PCR products were separated on a 2% agarose gel. Lane 1: 100-bp ladder; lane 2: negative control (without template); lane 3: RT-PCR result showing the 219-bp fragment of human β-actin amplified from the extracted RNA.

In the case of the highest flow rate (25 ml h^{-1}) used with the present RNA microextractor, the calculated Reynolds number was about 13. Thus, even at a high flow rate, the fluidic flow of the RNA microextractor is expected to be laminar.[27] Such laminar flow is crucial to obtaining a high-quality RNA sample because it allows a multi-stream fluid in which the beads are selectively transported across the sample and buffer stream boundary into outlet #1.

4.3 RT-PCR performance

RT-PCR, a method for detecting the presence of specific RNA, was performed using RNA extracted with the present RNA microextractor. As RNA bound to magnetic beads does not require elution for downstream application (*e.g.*, solid-phase cDNA synthesis and PCR), the isolated RNA was used directly in cDNA synthesis while still bound to the beads. A solution of 12.5 μl obtained from outlet #1 was used for synthesizing cDNA. After synthesis, PCR was performed using primers for amplification of a 219-bp fragment of human β-actin in a commercial thermocycler (PC808; Astec), followed by gel electrophoresis. Fig. 8 shows representative RT-PCR results. A negative control (lane 2) showed no amplified signal, while the RT-PCR using RNA isolated from blood lysate using the RNA microextractor showed the 219-bp product (lane 3). These results demonstrated the successful RT-PCR amplification of human β-actin using the extracted RNA preparation. This means that the purity of the RNA isolated by the RNA microextractor was of sufficient quality for use directly in subsequent genetic analysis procedures.

5. Conclusions

We presented the design, fabrication, and characterization of a high-speed RNA microextractor for isolating RNA from human blood lysate using magnetic oligo-dT beads and lateral magnetophoresis. Comparison between analytical and numerical simulations for magnetic forces verified that the analytical model

was effective for estimating the magnetic force on beads placed near the inlaid ferromagnetic wire. A permanent magnet, generating an external magnetic flux of 0.14 T, was used to create a high-gradient magnetic field around the inlaid ferromagnetic wire. The experimental results showed that the RNA microextractor continuously separated more than 80% of the magnetic beads from human blood lysate at sample flow rates up to 20 ml h^{-1}; notably, the procedure was completed in just 1 min. RNA spectrophotometric measurements showed that the absorbance ratio of RNA to protein (A_{260}/A_{280}) was > 1.7, indicating that the purity of the RNA preparation was sufficient for RT-PCR procedures. In addition, through subsequent cDNA synthesis and PCR with the extracted RNA preparation, we further verified that the microextractor was effective for RT-PCR.

Compared with conventional column-type RNA purification methods, which take about 1 h to complete,[28] require trained personnel, and may expose RNA to the outside environment causing contamination, the proposed RNA microextractor is extremely simple for extracting RNA from crude lysate and requires much less time (less than 1 min), due to its simplicity. RNA can be extracted continuously and simultaneously during sample injection into the microchannel and it is protected against exposure to the outside environment by the closed microchannel. For the subsequent RT-PCR processes (cDNA synthesis and PCR amplification), only 12.5 μl (or one eighth of the total extracted sample volume of 100 μl) of the solution extracted from outlet #1 was used. Thus, for a single RT-PCR analysis, both the time and amounts of reagents required can be reduced by eightfold because the sample volume is reduced.

We believe that the present RNA microextraction technology may provide a practical method for simple, rapid, and high-precision RT-PCR using minimal reagent volumes without the need for highly trained personnel. As the RNA microextractor can be readily integrated with other downstream functional compartments[29,30] (*e.g.*, cDNA synthesis and PCR), the RNA microextractor could be used for developing micro-scale automated platforms for genetic analysis systems, having the important advantages of being rapid, easy to use, and highly precise (Fig. S4†).

Acknowledgements

This work was supported by the Basic Science Research Program (Grant No. D00771) and by the Mid-career Researcher Program (Grant No. 2009-0083956) through the National Research Foundation (NRF) of Korea funded by the Ministry of Education, Science and Technology (MEST).

References

1 C.-S. Liao, G.-B. Lee, H.-S. Liu, T.-M. Hsieh and C.-H. Luo, *Nucleic Acids Res.*, 2005, **33**, e156.
2 T. Takano, A. Miyauchi, T. Yokozawa, F. Matsuzuka, G. Liu, T. Higashiyama, S. Morita, K. Kuma and N. Amino, *Cancer Res.*, 1998, **58**, 4913–4917.
3 S. Burchill, M. Bradbury, K. Pittman, J. Southgate, B. Smith and P. Selby, *Br. J. Cancer*, 1995, **71**, 278–281.
4 M. Setzer, J. Juusola and J. Ballantyne, *J. Forensic Sci.*, 2008, **53**, 296–305.
5 J. Juusola and J. Ballantyne, *Forensic Sci. Int.*, 2003, **135**, 85–96.
6 S.-I. Han, K.-H. Han, A. B. Frazier, J. P. Ferrance and J. P. Landers, *Biomed. Microdevices*, 2009, **11**, 935–942.
7 C. Zhang and D. Xing, *Nucleic Acids Res.*, 2007, **35**, 4223–4237.
8 Q. Wu, J. M. Bienvenue, B. J. Hassan, Y. C. Kwok, B. C. Giordano, P. M. Norris, J. P. Landers and J. P. Ferrance, *Anal. Chem.*, 2006, **78**, 5704–5710.
9 N. C. Cady, S. Stelick and C. A. Batt, *Biosens. Bioelectron.*, 2003, **19**, 59–66.
10 M. C. Breadmore, K. A. Wolfe, I. G. Arcibal, W. K. Leung, D. Dickson, B. C. Giordano, M. E. Power, J. P. Ferrance, S. H. Feldman, P. M. Norris and J. P. Landers, *Anal. Chem.*, 2003, **75**, 1880–1886.
11 K. A. Wolfe, M. C. Breadmore, J. P. Ferrance, M. E. Power, J. F. Conroy, P. M. Norris and J. P. Landers, *Electrophoresis*, 2002, **23**, 727–733.
12 K. A. Hagan, W. L. Meier, J. P. Ferrance and J. P. Landers, *Anal. Chem.*, 2009, **81**, 5249–5256.
13 K. A. Hagan, J. M. Bienvenue, C. A. Moskaluk and J. P. Landers, *Anal. Chem.*, 2008, **80**, 8453–8460.
14 K.-Y. Lien, J.-L. Lin, C.-Y. Liu, H.-Y. Lei and G.-B. Lee, *Lab Chip*, 2007, **7**, 868–875.
15 J. S. Marcus, W. F. Anderson and S. R. Quake, *Anal. Chem.*, 2006, **78**, 3084–3089.
16 J. S. Marcus, W. F. Anderson and S. R. Quake, *Anal. Chem.*, 2006, **78**, 956–958.
17 J. W. Hong, V. Studer, G. Hang, W. F. Anderson and S. R. Quake, *Nat. Biotechnol.*, 2004, **22**, 435–439.
18 G. Fonnum, C. Johansson, A. Molteberg, S. Mørup and E. Aksnes, *J. Magn. Magn. Mater.*, 2005, **293**, 41–47.
19 J. Jung and K.-H. Han, *Appl. Phys. Lett.*, 2008, **93**, 223902.
20 K.-H. Han and A. B. Frazier, *J. Microelectromech. Syst.*, 2005, **14**, 1422–1431.
21 K.-H. Han and A. B. Frazier, *J. Appl. Phys.*, 2004, **96**, 5797–5802.
22 N. Pamme, J. C. T. Eijkel and A. Manz, *J. Magn. Magn. Mater.*, 2006, **307**, 237–244.
23 J. D. Adams, U. Kim and H. T. Soh, *Proc. Natl. Acad. Sci. U. S. A.*, 2008, **105**, 18165–18170.
24 D. W. Inglis, R. Riehn, R. H. Austin and J. C. Sturm, *Appl. Phys. Lett.*, 2004, **85**, 5093–5095.
25 M. M. Hämäläinen, J. U. Eskola, J. Hellman and K. Pulkki, *Clin. Chem.*, 1999, **45**, 465–471.
26 J. Sambrook and D. W. Russell, *Molecular cloning: a laboratory manual*, 3rd edn, Cold Spring Harbor Laboratory Press, New York, 2001, Vol. 1.
27 L. Bousse, C. Cohen, T. Nikiforov, A. Chow, A. R. Kopf-Sill, R. Dubrow and J. W. Parce, *Annu. Rev. Biophys. Biomol. Struct.*, 2000, **29**, 155–181.
28 QIAGEN, *QIAamp® RNA blood mini handbook: For total RNA purification from human whole blood*. 2nd edn, 2006.
29 K.-H. Han, R. D. McConnell, C. J. Easley, J. M. Bienvenue, J. P. Ferrance, J. P. Landers and A. B. Frazier, *Sens. Actuators, B*, 2007, **122**, 337–346.
30 C. J. Easley, J. M. Karlinsey, J. M. Bienvenue, L. A. Legendre, M. G. Roper, S. H. Feldman, M. A. Hughes, E. L. Hewlett, T. J. Merkel, J. P. Ferrance and J. P. Landers, *Proc. Natl. Acad. Sci. U. S. A.*, 2006, **103**, 19272–19277.

